Defect and Diffusion Forum *Online: 2011-03-15*
ISSN: 1662-9507, Vol. 311, pp 137-158
doi:10.4028/www.scientific.net/DDF.311.137

TiO_2 Nanomaterials Studied by $^{44}Ti(EC)^{44}Sc$ Time Differential Perturbed Angular Correlations: Volume and Surface Properties

T. Butz[1,a], S.-b. Ryu[1], St. Jankuhn[1,b], S. K. Das[2], and S. Ghoshal[1,3]

[1] Universität Leipzig, Fakultät für Physik und Geowissenschaften,
Linnéstraße 5, 04103 Leipzig, Germany
[2] Variable Energy Cyclotron Centre, Bhabha Atomic Research Centre,
1/AF Bidhan Nagar, Kolkata 700064, India
[3] Bhabha Atomic Research Centre, Chemistry Division, Trombay, Mumbai 400 085, India

[a] butz@physik.uni-leipzig.de, [b] jankuhn@physik.uni-leipzig.de

Keywords: TiO_2 – TDPAC – Nanoparticles – Surface Properties – ^{44}Ti

Abstract. TiO_2 nanoparticles (anatase) with diameters between 2 and 4 nm were synthesized by controlled hydrolysis of a solution of titanium (IV)isopropoxide to which ^{44}Ti in 4*M* HCl was added. Inactive nanoparticles were analyzed by X-ray diffraction (XRD) and high resolution transmission electron microscopy (HRTEM), the active ones were analyzed by measuring the nuclear quadrupole interaction (NQI) of the $I = 1$ state in ^{44}Sc using time differential perturbed angular correlation (TDPAC). Rather broad distributions were obtained. We also synthesized nanowires with typical diameters of 2 nm and 100 nm length using shape controllers. They were analyzed by HRTEM and XRD. The material turned out to be TiO_2(B). The ^{44}Ti was added by impregnation and diffusion at 180°C for two hours. Two well-defined NQI signals were observed which we tentatively assigned to the "volume" fraction and the "surface" fraction, i.e. ^{44}Ti-probes with OH-termination. In addition, we studied AMT-100 (anatase, uncoated, 6 nm), Eusolex T-2000 (rutile, Al_2O_3-coated, $20\times20\times100$ nm^3, simethicone additive) and P25 (mainly anatase, uncoated, 20 nm diameter) using the impregnation and diffusion method. P25 and the isolated rutile fraction from P25 yield spectra which correspond to anatase and rutile volume signals plus their surface signals, respectively. TDPAC thus proved very useful in characterizing the nanomaterials, especially their disorder, by measuring the NQI. In addition, information on surface properties is obtained. The relatively narrow surface signals indicate a lower degree of disorder and are possibly also a result of partial motional averaging of Ti-signals with OH-bonds due to mobile H-atoms.

Introduction

Nanomaterials of TiO_2 are in use for various applications: as UV-filters in sunscreens, as photocatalysts for wastewater decomposition, in photovoltaics, in photo-/electrochromics, as sensors, and as intercalation host, e.g. for hydrogen storage [1]. The two important modifications are anatase and rutile with slightly different absorption edges. There is a further modification which thus far did not receive adequate attention, the TiO_2(B) modification, a metal oxide bronze [2]. All polymorphs are composed of Ti-O octahedra, which share edges and corners. Rutile is the high-temperature modification, which is metastable upon cooling. It consists of chains where all O-atoms share 3 Ti-atoms and the octahedra are connected via edges and corners. In anatase all O-atoms share 3 Ti-atoms and the octahedra are connected via edges and corners. TiO_2(B) has a layered structure, a covalent framework of bronzes, with four O-atoms sharing 4 Ti-atoms and 2 O-atoms sharing 2 Ti-atoms. This material can intercalate H or Li. It is important to note that the crystalline materials have a well-defined number of edge- and/or corner-sharing of octahedra. In fact, the above situations are the only ones where the charge neutrality is guaranteed in view of the fact that Ti is tetravalent and apparently prefers higher coordination numbers and thus tetrahedral O-coordination does not prevail.

These nanomaterials are usually characterized by XRD in order to obtain the crystal structure and to some extent the particle size using the Debye–Scherrer formula, and by HRTEM in order to obtain particle sizes and size distributions. Both methods are indispensible. However, the structural disorder in these materials is difficult to obtain. On the one side, the Bragg reflections are rather broad for particles with dimensions of 10 nm and below. A clear discrimination between amorphous and crystalline is possible but disorder is difficult to detect. On the other side, the observation of lattice fringes in HRTEM suggests good structural order or crystallinity; however, often it is the contrast due to lattice fringes, which makes the particles distinguishable from the background only. In other words, it is not clear whether the observation is representative. In addition, the observation of fringes does not exclude disorder, and atomic resolution is seldom achieved with the additional caveat that the mere sample preparation might modify the sample.

A rather crucial test for crystal perfection or disorder is the measurement of the NQI, e.g. at the metal site. The NQI is very sensitive to the first few coordination shells and point or extended defects, in particular disorder due to a mixture of edge- and corner-sharing octahedra, will inevitably show up in distributions of electric field gradients (EFGs). Thus, sharp frequencies or relatively sharp frequency distributions are a clear indication of good crystallinity, the opposite is true for broad distributions.

A naïve view of a nanoparticle is that it is the same material as its bulk counterpart but just smaller. This view is utterly wrong. For nanomaterials with dimensions in the range from 20 nm and below new and interesting phenomena will show up: those metal probes which are close to the surface will be coordinated by O-atoms which belong to the surface termination. For TiO_2 in air or water there will be an O-excess. In order to compensate this extra negative charge the surface can be OH-terminated through water dissociation as shown by ^{1}H-NMR studies [3]. This is the "chemists approach". In other words, the stoichiometry of the nanomaterial deviates from that of the bulk.

Internal O-vacancies or substoichiometric Ti-O-phases in order to compensate for the surface O-excess are not considered reasonable, certainly not for materials grown and heated in air. This is in contrast to single crystal surfaces, sputtered with Ar-ions in ultra-high vacuum, where bridging O-vacancies were observed [4]. We would also like to exclude the presence of Ti^{3+} with a nearby O-vacancy as has been observed by 2 MeV oxygen irradiated rutile single crystals [5], a treatment which leads to ferromagnetic order.

A closer look to the synthesis of the nanomaterials under conditions where protons are available, e.g. through dissociation of water, suggests that edge-sharing octahedra and corner-sharing octahedra with different connectivities can coexist and charge neutrality can be achieved by H-atoms. Thus natural intrinsic disorder could arise from a mixture of corner-sharing and edge-sharing octahedra for O-rich species. This would be the "physicists approach". A textbook example is the molybdenum oxide family, which is particularly rich because both octahedral and tetrahedral coordinations prevail and molybdenum is polyvalent. In other words, the surface O-excess could have far-reaching effects on the deeper parts of the nanomaterial.

Furthermore, for nanomaterials whose BET-surface area compared to the particle size is large, we expect pores, which in turn affect deeper parts of the nanomaterial.

As far as the photocatalytic properties of TiO_2 are concerned, a large mean free path of the electrons liberated by photo-absorption would be desirable in order to reach the surface where they can induce radical reactions, e.g. for waste water decomposition. In this respect, defects and disorder in the volume would be undesirable.

Apart from the "volume" NQI signal, which should resemble the value for the bulk but might be broadened substantially due to disorder, we expect a "surface" signal, which should become more pronounced for larger surface-to-volume ratios. For highly mobile H at the surface we expect sharp surface signals due to motional averaging, a dynamic property which has not been used thus far for the characterization of nanomaterials. In addition, the disorder at the surface might be less pronounced than in deeper parts of the material. In any case, the surface topology plays a crucial

role for the reactivity of the nanomaterial, as has been discussed recently in a combined scanning tunneling microscopy and first-principles calculation [6].

In this work we have first synthesized and characterized TiO_2 nanoparticles by XRD, HRTEM (inactive), and TDPAC (active). We then synthesized nanowires using shape-controllers, characterized them by XRD and HRTEM, and found out that it is possible to impregnate (a term which is commonly used in heterogeneous catalysis) these wires with ^{44}Ti in solution followed by diffusion at temperatures as low as 180°C (in heterogeneous catalysis this step would be called calcination, but usually is carried out in a different atmosphere and at much higher temperature). This opens up the possibility to use all commercial and well-characterized products for subsequent TDPAC studies. We studied AMT-100 (anatase, uncoated, 6 nm) from Tayca [7], Eusolex T-2000 (rutile, coated) from Merck [8], and P25 (predominantly anatase) from Degussa/Evonik [9] and a rutile extract thereof. In all cases except the rutile extract from P25 two signals were observed, the prominent one being associated with the volume fraction based on bulk data [10], whereas the extra fraction is ascribed to the probes closest to the surface. Various degrees of disorder were observed judging from observed linewidths.

Why did we use ^{44}Ti as the nuclear probe? At first glance, the TDPAC spectroscopy with this probe seems to be rather discouraging because of the small anisotropy of at best +4% [10]. In addition, the two lines of the cascade in the daughter ^{44}Sc are very close to each other and scintillators with a very good energy resolution are required in order to separate start and stop pulses which helps in improving the signal-to-noise ratio at large times. Finally, the quadrupole moment of the intermediate excited state is small and, hence, the observed NQI frequencies are small. The crucial advantages, however, are: (i) ^{44}Ti is a natural constituent of the sample and hence, by definition, a stable label for further studies on incorporation, translocation, accumulation, excretion in animals as well as for solubility studies; there is no question about the lattice location of this probe/label; (ii) the intermediate state in the cascade in ^{44}Sc is $I = 1$ which leads to rather simple perturbation functions, and above all, to an excellent sensitivity for small deviations from axial symmetry of the EFG tensor, contrary to systems with half-integer spins. It turned out that both properties are crucial for the interpretation of the spectra; (iii) the start level of the cascade in ^{44}Sc has a half-life of 51.1 μs, sufficiently long to allow for a complete re-arrangement of the Sc atomic shell.

Sample preparation and characterization

Inactive and ^{44}Ti-labelled nanoparticles. The method used is essentially that described by Bahnemann et al. [11]. A solution of 2.5 ml of titanium(IV)isopropoxide ($Ti(OCH(CH_3)_2)_4$) dissolved in 47.5 ml isopropyl alcohol was added dropwise to 450 ml of millipore water whose pH has been adjusted to 1.5–2.9 (see below) with HNO_3. During this process, the solution was continuously stirred. When the titanium(IV)isopropoxide and isopropyl alcohol solutions are added to pH 1.5 water, the formation of a white precipitate was immediately visible. The whole solution was kept stirred and left for approximately 12 h until the formation is complete. During the hydrolysis process, the temperature was controlled to be 275 K. Then the solution was concentrated by drying under N_2 gas running at 310 K to give a white powder. The crystallite size of the final product depends on the pH value of the solution. Three sets of samples were produced under pH = 1.5, pH = 2.1, and pH = 2.9.

The preparation of the ^{44}Ti-labelled nanoparticles was done in a slightly different way. The reason was that ^{44}Ti was available in a 4*M* HCl solution and adding this in the above process would alter the pH significantly. Therefore we dried up the solution first and took it up again with a known amount of HNO_3, which then was used as buffer solution of known pH.

The XRD data of these three nanoparticle samples are shown in Fig. 1. The prominent reflection at $2\theta = 25°$ and the other reflections clearly show that the nanoparticles have the anatase structure. No annealing was performed because annealing would increase the crystallite size [12,13]. The particle size was deduced from the peak width using the Debye–Scherrer formula:

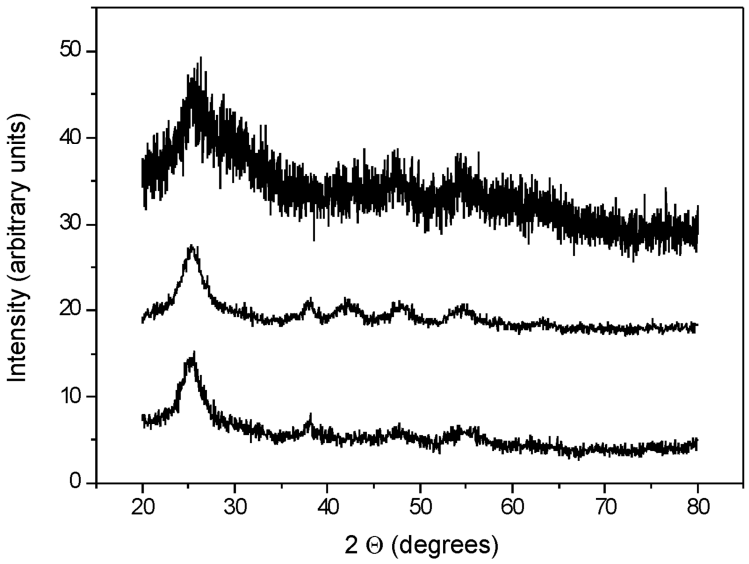

Fig. 1: XRD data for the nanoparticles produced at pH = 1.5 (top), pH = 2.1 (middle), and pH = 2.9 (bottom).

$$D = k\lambda / \beta\cos\theta \qquad (1)$$

with k the Scherrer constant (0.9 for spherical particles), λ the wavelength, β the full width at half maximum of the Bragg peak, and θ the position of Bragg peak. We obtained particle sizes of 2.1(1.1) nm, 3.2(1.4) nm, and 4.3(2.1) nm for the particles produced at pH = 1.5, pH = 2.1, and pH = 2.9, respectively. The uncertainties in these quantities are large. In Fig. 2 a bright field HRTEM image is shown for the 2.1 nm particles together with a histogram of the size distribution. For comparison, the size distribution deduced from XRD is also shown. There is good agreement between both size determinations.

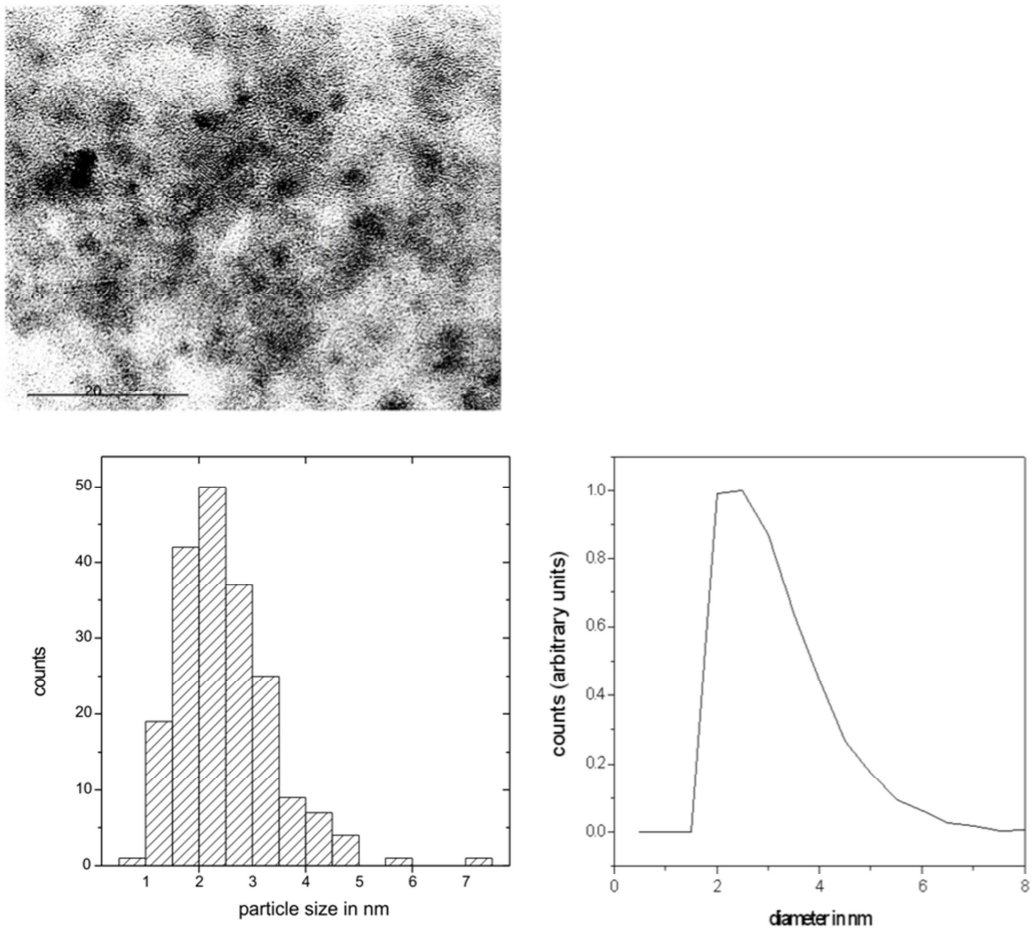

Fig. 2: HRTEM bright field image of 2.1 nm TiO_2-particles (top); scale bar is 20 nm; lattice fringes with 0.34–0.37 nm are visible. Histogram of particle size distributions derived from HRTEM (bottom left). Size distribution derived from XRD (bottom right).

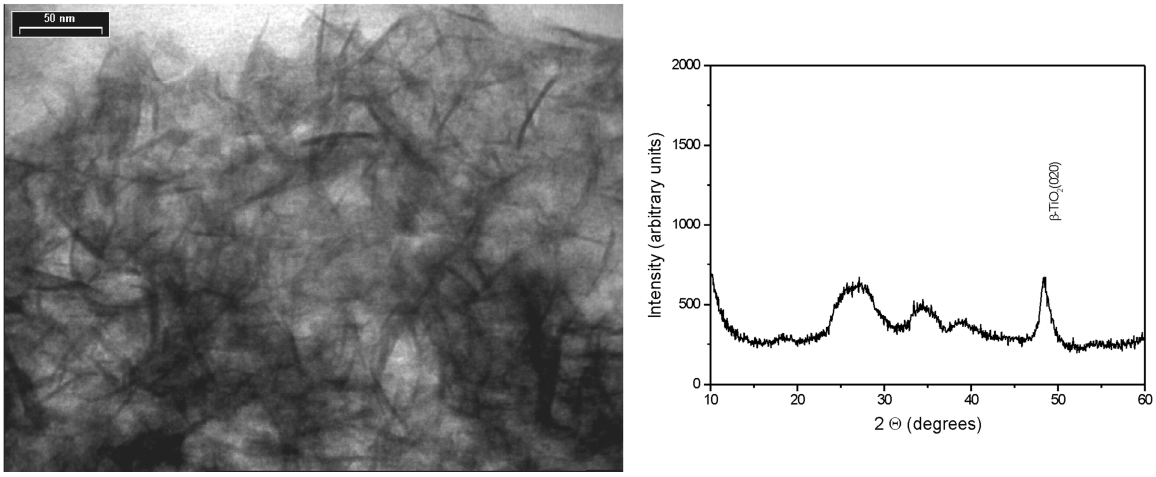

Fig. 3: TEM of TiO_2 nanowires (left); XRD of TiO_2 nanowires (right).

Inactive Nanowires and diffusion of ^{44}Ti. For the preparation of nanowires we essentially followed the prescription of Songwang Yang and Lian Gao [14] for the preparation of nanorods using shape controllers. In a 50 ml round bottom flask, (3 ml, 0.03*M*) aqueous titanium tetrachloride solution (prepared immediately before use from 3*M* $TiCl_4$) was added to 6 ml of isopropanol in an ice water bath. To this reaction mixture 1 ml of ethylenediamine was added. The reaction mixture was then allowed to stir for 30 min. The obtained suspension was then transferred to a quartz ampoule, frozen with the help of liquid nitrogen and then sealed. The suspension was then annealed at 180ºC for 30 h in a furnace. The only difference between [14] and our method was that we used a quartz tube instead of a steel autoclave lined with teflon. The white precipitate formed was then filtered out in a Whatman filter paper and washed several times with ethanol. It was then dried at 60ºC overnight under vacuum to get a white powder. The product obtained was then characterized by XRD and HRTEM. Figure 3 left shows nanowires with typical diameters of 2–4 nm and lengths

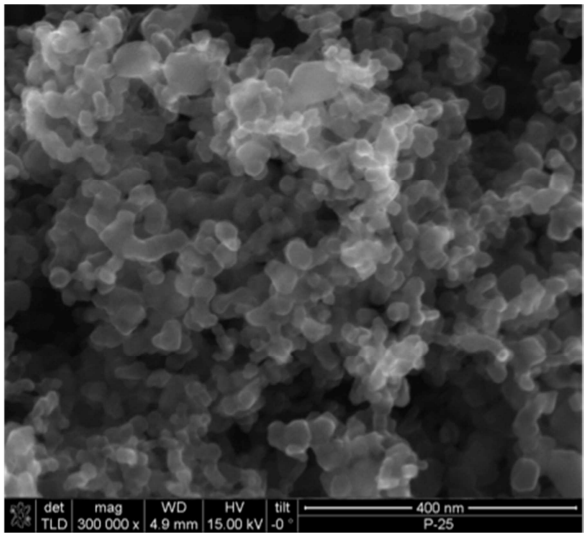

Fig. 4: SEM-image of P25 (mainly anatase approx. 20 nm).

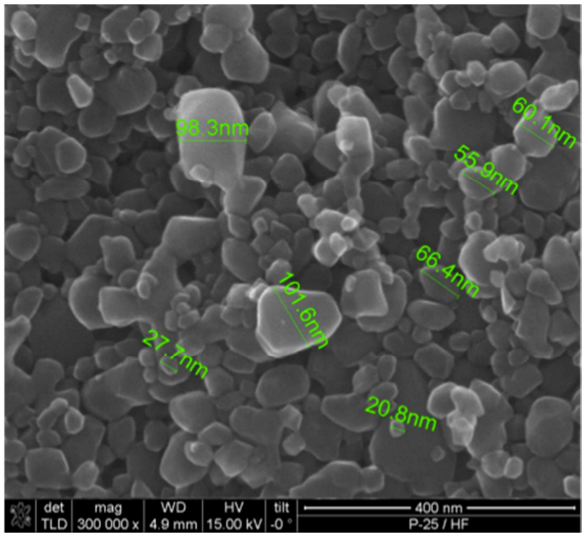

Fig. 5: SEM-image of the rutile-extract from P25 (20–100 nm).

up to 100 nm. The wires are slightly bent. Figure 3 right shows the XRD pattern with rather broad reflections except the relatively sharp (020) reflection which is a pure reflection along the *b*-axis, the long wire axis, for the TiO_2(B) modification (sometimes called β-TiO_2 or bronze). We believe that the nucleation at the quartz surface might be the cause for the different modification and smaller diameters compared to [14].

After characterization of the nanowires we impregnated them with 10–50 µl of carrier-free ^{44}Ti in 4*M* HCl, dried at 300 K to 330 K and diffused the label at 180°C for 2 h. We were reluctant to go to higher temperatures because we expected sintering to occur. At first glance, this temperature seems to be too low for diffusion. However, one should keep in mind that for 2–4 nm diameters there are a few lattice spacings only which the label must diffuse for homogeneous doping. We also tried to prepare the nanowires with the carrier-free ^{44}Ti in 4*M* HCl directly added to the solution. However, the results were discouraging, probably due to side reactions with the organic material, and were not pursued further.

Diffusion of ^{44}Ti in commercial products. Encouraged by the success with ^{44}Ti impregnation and diffusion we applied the same procedure to AMT-100 (anatase 6 nm uncoated, BET-surface 280 m^2/g) by Tayca [7]. In order to be sure that 2 h diffusion at 180°C was sufficient, we diffused the label in the same sample again for 22 h and found no change in the TDPAC spectra. Hence, 2 h was already sufficient.

Next we used Eusolex T-2000 [8] with the following properties according to the technical data sheet: modification rutile, primary particle size < 20 nm, lanceolate shape, coated with Al_2O_3 (content 8–11%), BET-surface 70–120 m^2/g, simethicone as additive (1–3% SiO_2). Again we diffused the label for 2 h at 180°C. We did not expect to encounter problems due to the added simethicone because of its low level. However, the Al_2O_3 coating could affect the diffusion. It would in any case modify the surface properties.

Next we used P25 [9] with the following properties according to the data sheet and [15]: 75% anatase with 25 nm primary particle size and 25% rutile with 85 nm primary particle size, uncoated, BET surface 49.2 m^2/g. Figure 4 shows a scanning electron microscopy (SEM) image of this product. We diffused the label for 2 h at 180°C.

Finally, we extracted the pure rutile component from P25 using 10% HF according to the prescription of [15]. As can be seen in Fig. 5 the morphology of the extract is quite different from the anatase component in P25. Particle diameters range from 100 nm down to 20 nm, approximately. We diffused the label for 27 h at 180°C.

TDPAC spectroscopy

The Ti-isotope used has a ɣ-ɣ-cascade with energies of 68 keV and 78 keV, respectively (see Fig. 6). The measurement was carried out at room temperature using a TDPAC camera with six $LaBr_3$(Ce) detectors of 12 mm diameter and 12 mm height, hence obtaining a total of thirty coincidences. These detectors have a good energy resolution and the 68 keV and 78 keV lines can just be resolved (see Fig. 7).

The lower half of the 68 keV peak and the upper half of the 78 keV were selected so that we do not get leakage for negative times. As expected, leakage was not observed in the TDPAC spectra obtained. This leads to a reduction in the uncorrelated background, which is particularly important for low frequencies as in this study. The activity of the sample was quite weak (approx. 100 kBq) and the measurement was carried out over two to three weeks for each spectrum obtained. This allows to obtain better signal to noise ratios at large observation times compared to using a high activity with short data collection time. Later we used 38 mm diameter and 38 mm high $LaBr_3$(Ce) scintillators which improved the coincidence count rate by a factor of 20.

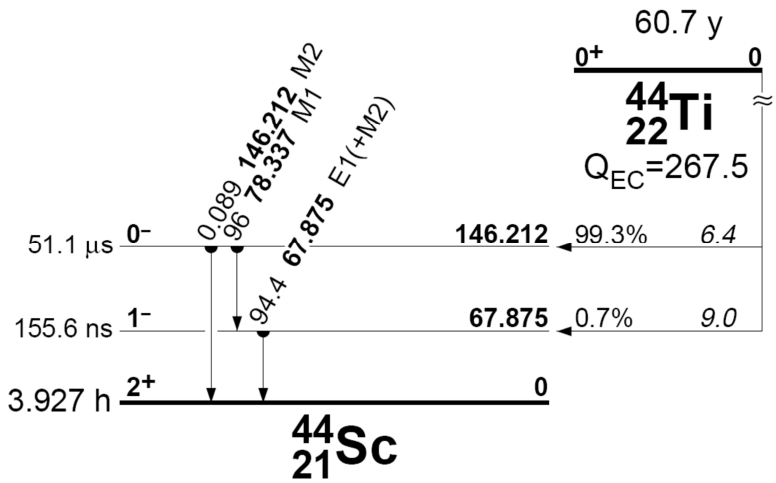

Fig. 6: Decay scheme of ^{44}Ti after [16] (the half life has been re-determined to be 60.7 y [17]).

The intermediate state in the daughter nuclide ^{44}Sc has a nuclear spin I = 1. This leads to a splitting with eigenvalues of $E_1 = 1+\eta$, $E_2 = 1-\eta$ and $E_3 = -2$ in units of the frequency $\omega_Q = eQV_{zz}/4\mathrm{h}$, where Q = ±0.214(3) b [10] is the nuclear quadrupole moment and V_{zz} is the largest component of the EFG tensor in magnitude. The powder perturbation function for the case I = 1 reads [18]:

$$G_{22} = \frac{2}{5} + \frac{1}{5}\cos(\omega_1 t) + \frac{1}{5}\cos(\omega_2 t) + \frac{1}{5}\cos(\omega_3 t) \qquad (2)$$

with $\omega_1 = 2\eta\omega_Q$, $\omega_2 = (3-\eta)\omega_Q$, $\omega_3 = (3+\eta)\omega_Q$, and $\eta = (V_{xx} - V_{yy})/V_{zz}$, the asymmetry parameter.

For frequency distributions each cosine-term (but not the hardcore, i.e. the time independent part in (2)) is multiplied by an exponential factor of the form $\exp(-\delta_i\omega_i t)$ with δ_i denoting the relative width of the (assumed) Lorentzian frequency distribution. In all cases we assumed line-distributions with a distribution in ω_Q and a sharp value for η. This will be justified as follows.

First, note that for small non-zero asymmetry parameters a low frequency emerges from the hardcore because the ±m degeneracy is lifted. In the time domain, this leads to a "sloping" baseline, i.e. the first fraction of a low frequency cosine is superimposed to all other features. In the frequency domain, the zero-frequency peak due to the hardcore starts to broaden for small η and eventually the frequency ω_1 separates from the zero-frequency peak. Thus, we are extremely sensitive to small η.

Next, 2D-distributions of EFG tensor components have to be discussed. For TiO_2(B) we have relatively sharp and well separated spectral features which do not require further explanations. The situation is different for anatase and rutile.

A simple distribution model for anatase is the wedge-shaped distribution osculating the upper boundary of the Czjzek-plot [19] as discussed in [20]. The corresponding perturbation function given in Eq. (24) of [20] leads to a sloping baseline as can be seen by using the trigonometric identity $\cos^2\alpha = ½(1 + \cos(2\alpha))$ for the last term in this equation. Hence, in this case, too, a sloping baseline would show up which would broaden the zero-frequency peak even for otherwise

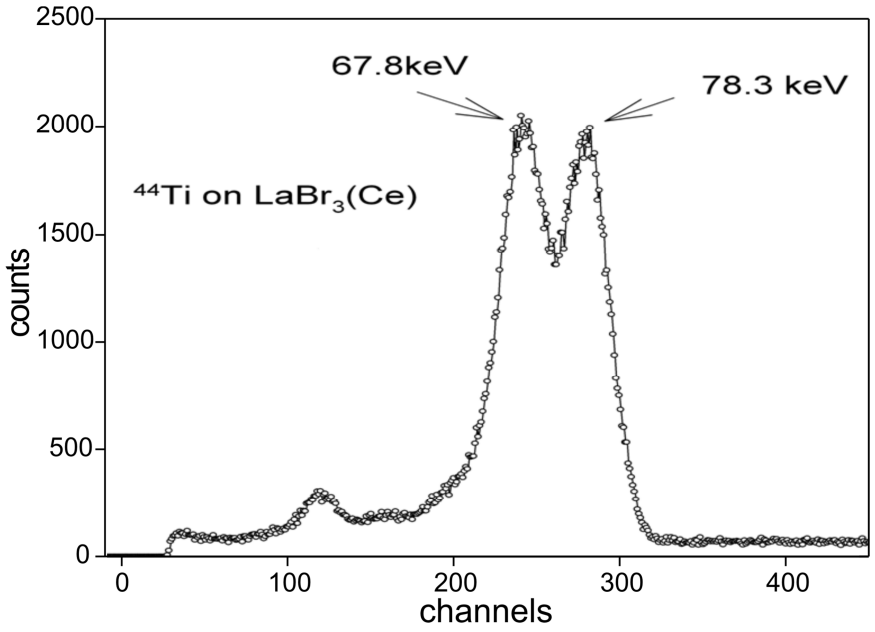

Fig. 7: γ-spectrum for ^{44}Ti using $LaBr_3(Ce)$ scintillators (after [10]).

very broad spectral features. If this is not the case, we have a line-distribution with $\eta = 0$, or at least a very small η.

A simple distribution model for anatase is the wedge-shaped distribution osculating the upper boundary of the Czjzek-plot [19] as discussed in [20]. The corresponding perturbation function given in Eq. (24) of [20] leads to a sloping baseline as can be seen by using the trigonometric identity $\cos^2 \alpha = ½(1 + \cos(2\alpha))$ for the last term in this equation. Hence, in this case, too, a sloping baseline would show up which would broaden the zero-frequency peak even for otherwise very broad spectral features. If this is not the case, we have a line-distribution with $\eta = 0$, or at least a very small η.

A simple distribution model for rutile is the wedge-shaped distribution osculating the lower boundary of the Czjzek-plot [19] as discussed in [20]. In this case there is no sloping baseline. However, as Eq. (26) of [20] shows, there are two spectral components with amplitudes 2:1 and frequencies ω_1 and $\omega_2 = 2\omega_1$ with different damping factors. There is an additional damping factor for ω_1 compared to ω_2, in other words the line width of the lower frequency peak would be larger than that for the harmonic. As will be shown below in the decomposition of the spectra, such patterns were never observed for rutile nanoparticles. Admittedly, the wedge-shaped distributions are crude model distributions leading to oscillations because of the sharp cut-off, but the essential features would remain the same for any more physical (and smoother) distribution functions.

The volume signal for Eusolex T-2000 has an η significantly lower than 1 and in this case a 2D-distribution cannot be excluded. For the rutile extract of P25 all spectral features were reasonably sharp and the question about the exact nature of the distribution function does not arise.

All time spectra were cosine-transformed for the sake of clarity and completeness.

Since the daughter of ^{44}Ti, namely ^{44}Sc, is a positron emitter, there is a 511 keV annihilation line whose Compton background causes prompt events in the 180°-spectra. Hence, the first few channels in the time spectra are corrupted and were excluded in the least-squares fit analysis.

In all original TDPAC spectra we fitted a constant baseline in the order of a percent or less which accounts for a non-perfect cancellation of detector efficiencies and imprecise sample

positioning. In the decomposition into individual fractions this baseline was subtracted. Data were recorded with 1.95 ns/channel and compressed once or twice, depending on the observed frequency.

None of the spectra exhibited a unique site signal. On the contrary, two or more sites were detected. The assignment of the lines was facilitated by the fact that in most cases the dominant fraction frequency was close to the known bulk value. Thus the start value for this fit parameter was easily found. In most cases a high-frequency shoulder was visible in the cosine-transforms which immediately gave a good start value for the second prominent component. It helped that this was generally less broadened than the prominent component. In many cases this second spectral component was higher than a factor of 2 than the prominent component, thus it could not belong to the same site (see Eq. (2)). In some cases, a clear deviation from axial symmetry was observed. In this case it greatly helped to decompose the spectra into individual subspectra. For intermediate values of η there must be three lines (the highest frequency must be the sum of the lower two), and moreover, of equal intensity. If this was not the case, the fit was discarded, despite an acceptable value for χ^2. A fit was considered satisfactory when all subspectra had correct perturbation functions in all respects. It always turned out that this also gave the smallest χ^2 globally.

TDPAC results

Anatase nanoparticles (2–4 nm). The TDPAC spectra with their cosine-transforms for the anatase nanoparticles with diameters between 2 and 4 nm are shown in Fig. 8. The spectra for the three different preparations with varying particle sizes were added because they did not show significant

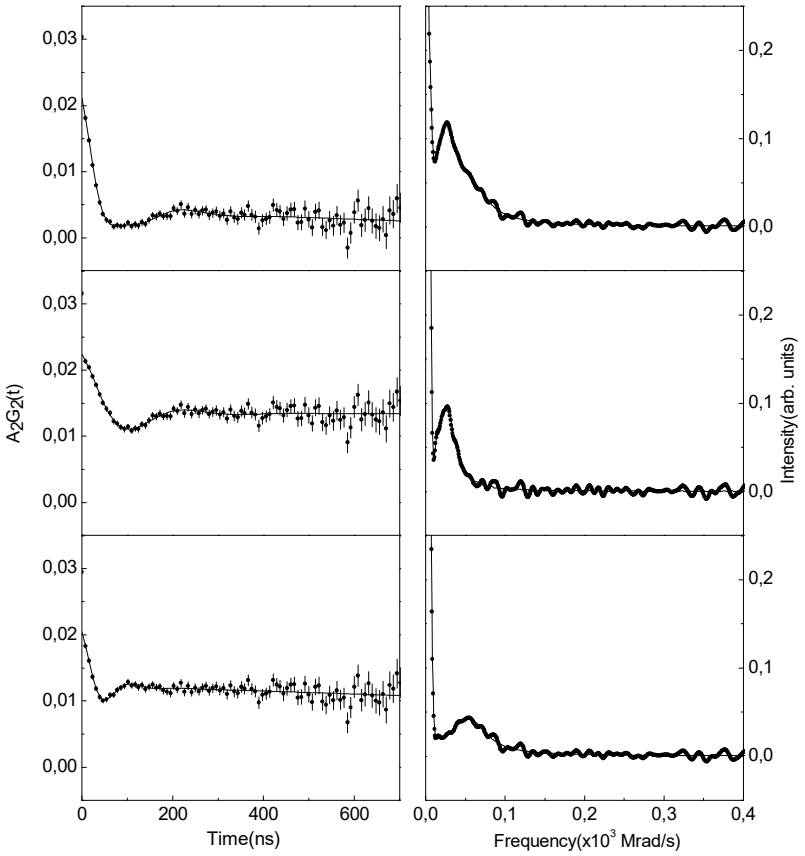

Fig. 8: Time spectra (left) and cosine-transforms (right) for anatase nanoparticles of 2–4 nm; top: total spectrum; middle: slow component; bottom: fast component.

differences. The solid line in the time spectrum is the result of a fit with the following two components: the first component has a frequency $\omega_{Q,1} = 8.7(6)$ Mrad/s and a Lorentzian damping $\delta_1 = 46(20)\%$, the second component has a frequency $\omega_{Q,2} = 18(2)$ Mrad/s and a Lorentzian damping $\delta_2 = 47(22)\%$. For the volume fraction η_1 was fixed to 0 because a fit with free η yielded zero with error bars of the order of 0.002. In other words, the zero-frequency peak was instrumentally sharp. The surface fraction exhibited a small deviation from axial symmetry. Both components have the same fraction within – admittedly – large error limits. The damping is rather large for both components. All fit parameters for this and all other materials are listed in Table 1. In Fig. 8 both components are also shown separately. The solid lines represent the fitted theoretical functions and their cosine-transforms. There is no indication of larger deviations from axial symmetry.

Nanowires. The TDPAC spectra with their cosine-transforms for the TiO_2(B) nanowires (2–4 nm diameter, up to 100 nm length) are shown in Fig. 9. The solid line in the time spectrum is the result of a fit with the following two components: the first has a frequency $\omega_{Q,1} = 10.2(2)$ Mrad/s and a Lorentzian damping $\delta_1 = 26(3)\%$, the second has a frequency $\omega_{Q,2} = 21.6(2)$ Mrad/s and a Lorentzian damping $\delta_2 = 4.5(9)\%$. For both components we fixed η to 0 because fits with free η gave values below 0.02 and larger error bars. The first component has a fraction $f_1 = 73(4)\%$ whereas the second has $f_2 = 27(4)\%$. Note the small damping, especially for the

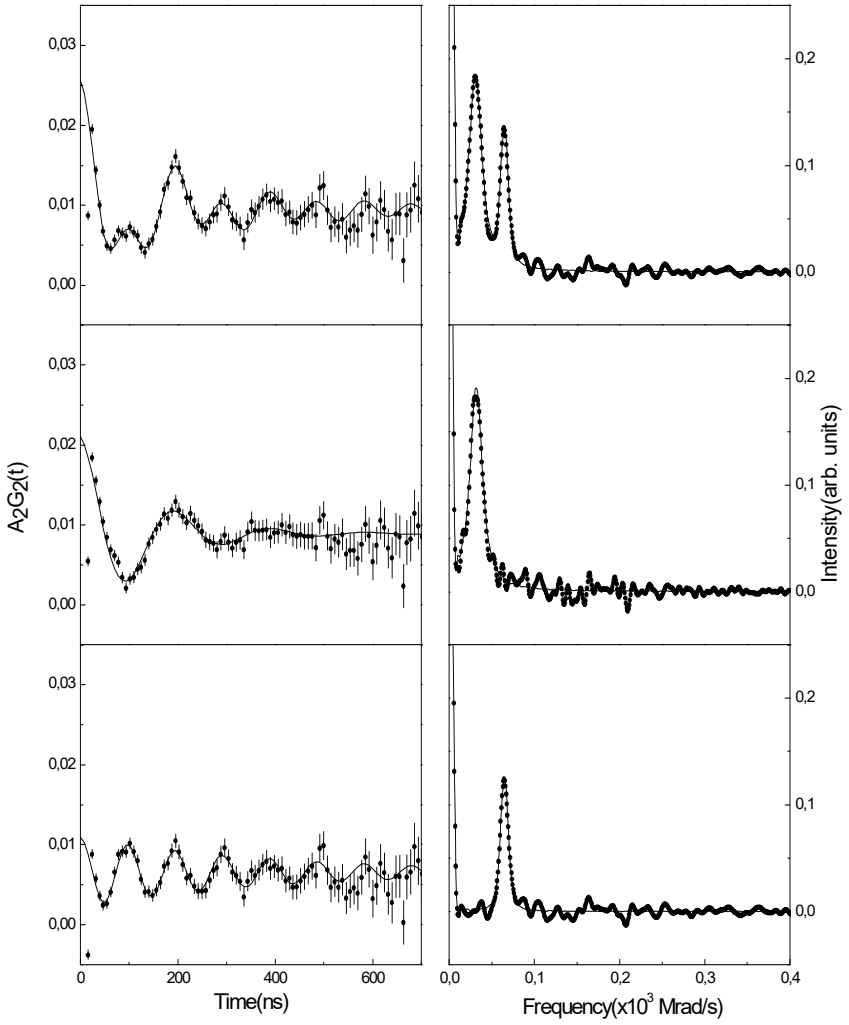

Fig. 9: Time spectra (left) and cosine-transforms (right) for TiO_2(B) nanowires; top: total spectrum; middle: slow component; bottom: fast component.

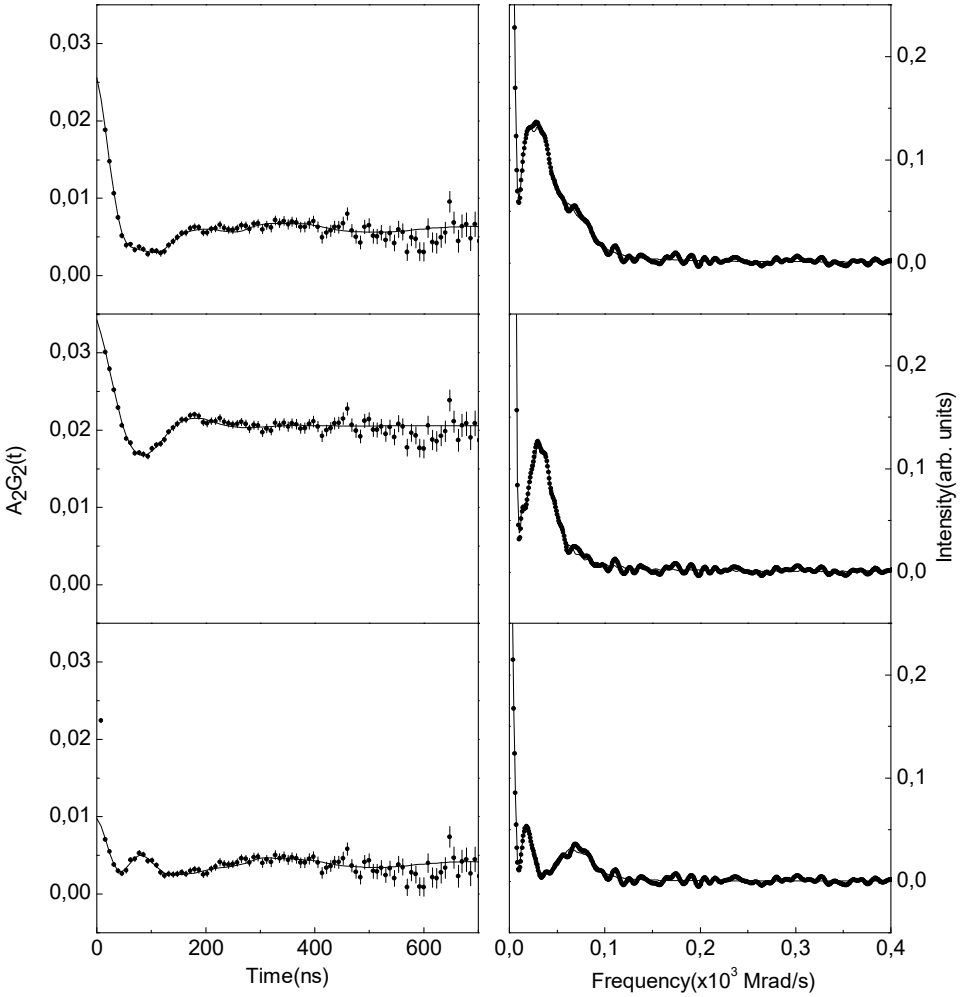

Fig. 10: Time spectra (left) and cosine-transforms (right) for AMT-100; top: total spectrum; middle: slow component; bottom: fast component.

second component. In Fig. 9 both components are also shown separately. It is clear that the higher frequency cannot be the harmonic of the lower one because the frequency ratio exceeds 2, the linewidth is too sharp, and the intensity would be wrong. Hence, there is no indication of a non-zero asymmetry parameter.

Commercial products – AMT-100 (anatase). The TDPAC spectra with their cosine-transforms for this product are shown in Fig. 10. The solid line in the time spectrum is the result of a fit with the following two components: the first has a frequency $\omega_{Q,1}$ = 10.9(1) Mrad/s and a Lorentzian damping δ_1 = 43(4)%, the second has a frequency $\omega_{Q,2}$ = 23.8(7) Mrad/s and a Lorentzian damping δ_2 = 16(5)%. For the first component we fixed η to 0 because a fit with free η gave 0.00004 with larger error bars whereas for the second component we fitted η_2=0.38(1). The first component has a fraction f_1 = 78(6)% whereas the second has f_2 = 22(6)%. Note the relatively small damping for the second component. In Fig. 10 both components are also shown separately. It is clear that a rather low frequency, weakly damped, is required in order to obtain a decrease of the anisotropy after about 375 ns with a subsequent increase. Hence, there is a clear indication of a non-zero asymmetry parameter for the second component

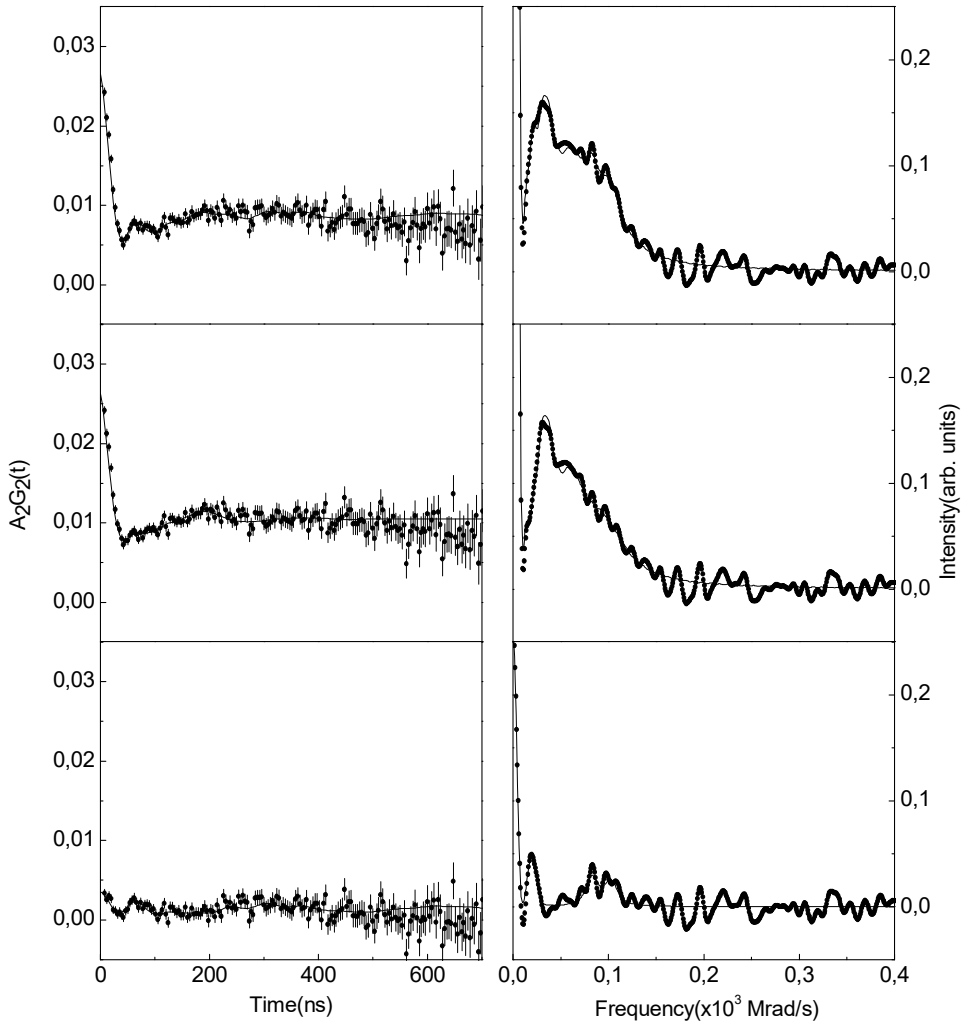

Fig. 11: Time spectra (left) and cosine-transforms (right) for Eusolex T-2000; top: total spectrum; middle: slow component; bottom: fast component.

Commercial products – Eusolex T-2000 (rutile). The TDPAC spectra with their cosine-transforms for the Eusolex T-2000 are shown in Fig. 11. The solid line in the time spectrum is the result of a fit with the following two components: the first has a frequency $\omega_{Q,1}$ = 25.9(1.0) Mrad/s and a Lorentzian damping δ_1 = 29(3)%, the second has a frequency $\omega_{Q,2}$ = 30.7(8) Mrad/s and a Lorentzian damping δ_2 = 6(4)%. For the first component we fitted η_1 = 0.64(2) whereas for the second component we fitted η_2 = 0.32(2). The first component has a fraction f_1 = 88(4)% whereas the second has f_2 = 12(4)%. Note the relatively small damping for the second component. In Fig. 11 both components are also shown separately. Again, a rather low frequency, weakly damped, is required in order to obtain a decrease of the anisotropy after about 375 ns with a subsequent increase. This is what the second component provides whereas the first component is too strongly damped.

Commercial products – P25 rutile-extract. The TDPAC spectra with their cosine-transforms for the pure rutile-extract from P25 are shown in Fig. 12. The solid line in the time spectrum is the result of a fit with the following four components: the first component has a frequency $\omega_{Q,1}$ = 17.2(3) Mrad/s and a Lorentzian damping δ_1 = 17(2)%, the second component has a frequency $\omega_{Q,2}$ = 26.3(3) Mrad/s and a Lorentzian damping δ_2 = 2(2)%, the third component has a frequency $\omega_{Q,3}$ = 23.6(7) Mrad/s and a Lorentzian damping δ_3 = 17(7)%, and the fourth component has a frequency $\omega_{Q,4}$ = 24.8(2) Mrad/s and a Lorentzian damping δ_4 = 2(1)%. For the first component we fitted η_1 = 0.81(2), for the second component we fitted η_2 =0.64(2), for the third component we fitted η_3 =0.04(1) , and for the fourth component we fitted η_4 = 0.37(1). The first component has a fraction f_1 = 60(10)%, the second has f_2 = 6(5)%, the third component has a

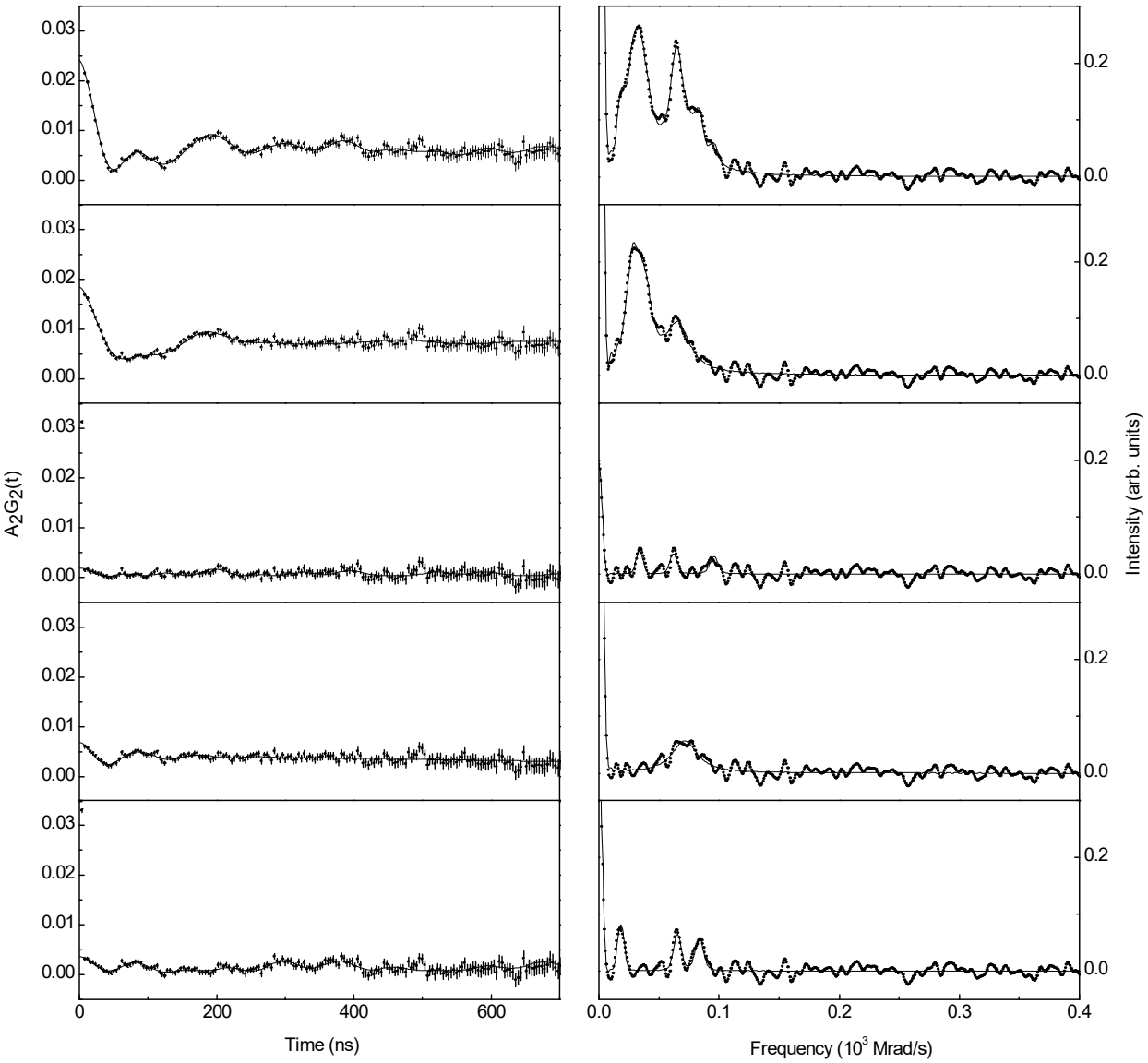

Fig. 12: Time spectra (left) and cosine-transforms (right) for the P25 rutile-extract; from top to bottom: total spectrum, spectrum for volume fraction of large particles, associated surface fraction, spectrum for volume fraction of small particles, associated surface fraction.

fraction f_3 = 22(9)%, and the fourth component has a fraction f_4 = 12(4)%. Note the small dampings for the second and fourth components. In Fig. 12 all components are also shown separately. As shown in Fig. 5 we expect NQI parameters close to those of bulk rutile for the large particles, as was indeed observed. This helped a great deal in the decomposition of the spectrum. As can be seen from the error bars, the fraction f_2 is close to the detection limit and not essential.

Commercial products – P25 (75% anatase, 25% rutile). The TDPAC spectra with their cosine-transforms for the original P25 are shown in Fig. 13. It is immediately clear that the majority fraction (anatase) must lead to a rather broad signal because most of the anisotropy is lost rapidly. For the analysis we used the results for the rutile-extract of P25 as fixed input with 25% fraction of the rutile volume and surface signal. Hence, we fitted signals for anatase only. The solid line in the time spectrum is the result of a fit with the following additional two components: the first has a frequency $\omega_{Q,1}$ = 9.6(7) Mrad/s and a Lorentzian damping δ_1 = 109(205)%, the second has a

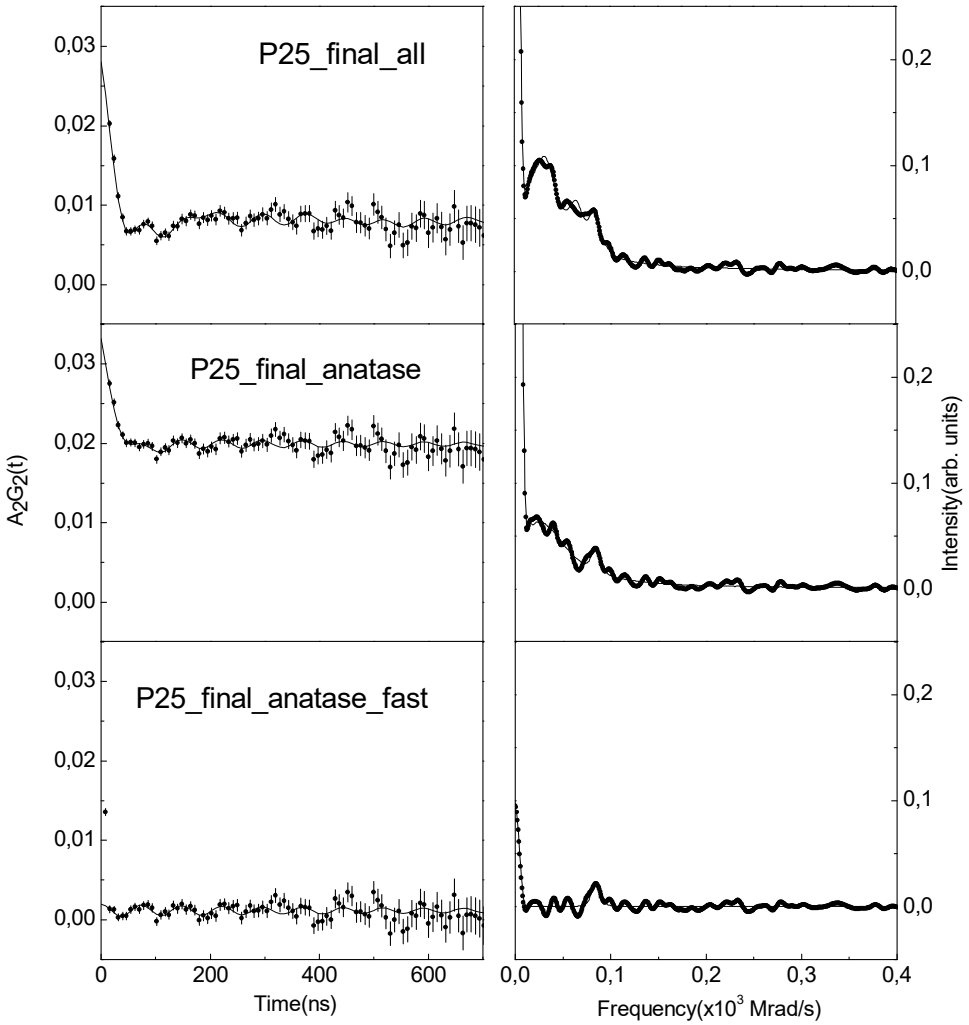

Fig. 13: Time spectra (left) and cosine-transforms (right) for original P25; top: total spectrum; middle: anatase slow and fast components, i.e. rutile fractions subtracted; bottom: anatase fast component.

frequency $\omega_{Q,2}$ = 28.3(5) Mrad/s and a Lorentzian damping δ_2 = 2(2)%. For both components we kept η = 0 fixed because the fit with free η's gave values below 0.05 with even larger error bars. The first component has a fraction f_1 = 70(6)% whereas the second has f_2 = 4.4(2.5)%. Note the small damping for the second component. On the contrary, the main component is excessively broadened. In Fig. 13 both components after subtraction of the rutile-extract of P25 components are also shown separately as well as the fast anatase component alone.

Summary of results. In Fig. 14 all observed signals for the volume fractions are displayed in a Czjzek-plot [19] for the sake of clarity. The data for anatase and TiO_2(B) are all very close together with η = 0 or very nearly so and correspond in increasing order of ω_Q to nano2_4, anatase bulk, P25_anatase, wires, AMT-100. Note that the size of the data points is generally larger than the uncertainty in η.

The data point with the largest η is for rutile bulk, the adjacent point for large rutile nanoparticles from the P25-extract. The rightmost point is for Eusolex T-2000 and the uppermost point is for small rutile nanoparticles from the P25-extract. The last two points are somehow outliers and belong to the small rutile category with different morphologies. A similar plot for the surface signals is not more instructive than the ratio ω_2 / ω_1 for the surface to volume signal quoted in Table 1, i.e. it has a value between approximately 2 and 3 for anatase and TiO_2(B), a value of 1.5 for large rutile nanoparticles from P25-extract, and approximately 1 for small rutile nanoparticles (Eusolex T-2000 and P25 rutile-extract).

Table 1: Fractions f in %, frequency ω_Q in Mrad/s, Lorentzian damping δ in %, asymmetry parameter η for the volume and surface sites (small δ) and ratio of surface/volume frequencies $\omega_{Q,2} / \omega_{Q,1}$ for various nanomaterials. The entries are ordered according to their structure. Bulk values for anatase and rutile are listed for reference purposes. "f" after a number means that this parameter was kept fixed in the least squares fit. For P25_rutile there are two volume and surface signals for large and small particles, respectively. For the P25_anatase data the 25% rutile fractions as obtained from P25_rutile were subtracted.

Sample	f_1	$\omega_{Q,1}$	δ_1	η_1	f_2	$\omega_{Q,2}$	δ_2	η_2	$\frac{\omega_{Q,2}}{\omega_{Q,1}}$	Ref.
Wires	73(4)	10.2(2)	26(3)	0f	27(4)	21.6(2)	4.5(9)	0f	2.12	this work
Nano2_4	52(32)	8.7(6)	46(20)	0f	48(32)	18(2)	47(22)	0.023(18)	2.07	this work
AMT-100	78(6)	10.9(1)	43(4)	0f	22(6)	23.8(7)	16(5)	0.38(1)	2.18	this work
P25_anatase	70(6)	9.6(7)	109(20)	0f	4.4(2.5)	28.3(5)	2(2)	0f	2.95	this work
P25_rutile	60(10)	17.2(3)	17(2)	0.81(2)	6(5)	26.3(3)	2(2)	0.64(2)	1.53	this work
	22(9)	23.6(7)	17(7)	0.04(1)	12(4)	24.8(2)	2(1)	0.37(1)	1.05	
T-2000	88(4)	25.9(1.0)	29(3)	0.64(2)	12(4)	30.7(8)	6(4)	0.32(2)	1.19	this work
Anatase Bulk	100	9.23(3)	8.4(8)	0.10(1)						[10]
Rutile Bulk	100	16.14(6)	0.3(5)	0.94(1)						[10]

Discussion

General remarks. For reference purposes we also list the hyperfine parameters for anatase bulk and rutile [10] in Table 1. Unfortunately, we do not have bulk data for TiO_2(B). The NQI for anatase is significantly lower than that for rutile, certainly a consequence of the different volume per unit cell and atom. Whereas for anatase we have axial symmetry, the NQI in rutile is almost antiaxial. For the larger nanomaterials we expect NQI parameters close to those of the bulk materials, eventually accompanied by a small surface signal.

Of course, deviations from the bulk values are expected the smaller the particles are. This simply follows from the fact that the stoichiometry of the materials is changed from TiO_2 (bulk) to $(1\text{-}x)TiO_2+xTi(OH)_4$ or $TiH_{4x}O_{2+2x}$.The hydrogen of the surface termination is considered highly mobile for smooth surfaces. For very small nanoparticles in the range from 2–4 nm the ratio of surface to volume fraction is roughly 1 (details depend on polymorph and morphology) and for 85 nm particles we expect to see the bulk signal with at best a few percent surface signal only. All subsequent estimates of surface to volume fractions should be taken with great precautions because the surface topology is essentially unknown.

In the following we address the following questions before discussing the individual nanomaterials:

i. What is the reason for the rather large linewidth of the volume signal?
ii. Why is the volume signal for nanowires so much sharper compared to rutile and anatase?
iii. Why is the surface signal in general much sharper than the volume signal?
iv. Why is there such a large deviation of the volume signal for small rutile particles compared to their larger counterparts and the bulk?

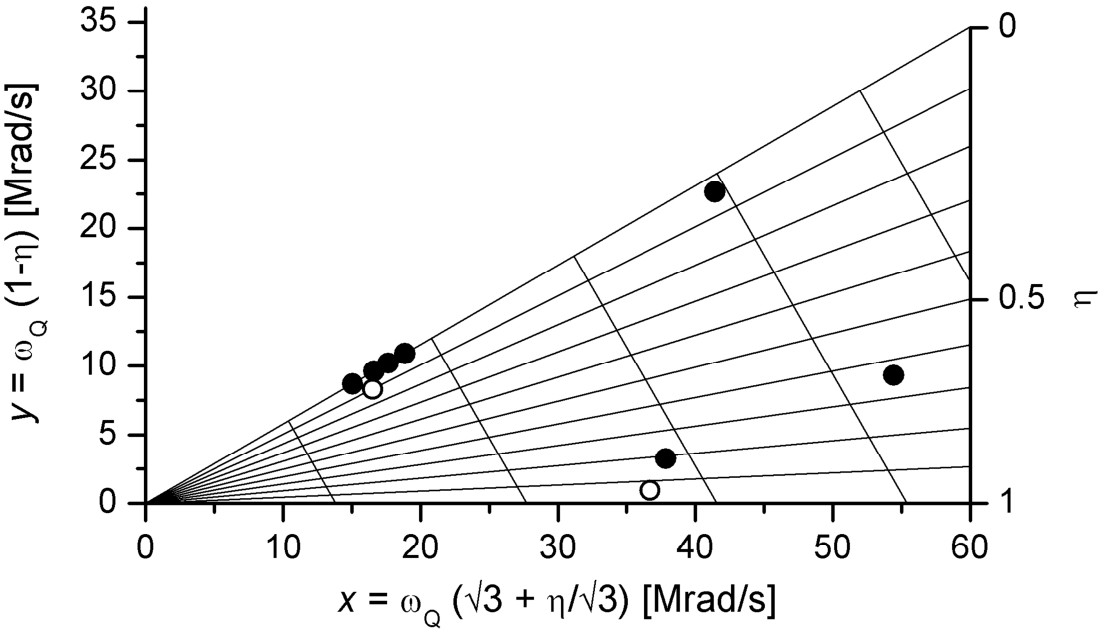

Fig. 14: Czjzek-plot showing all observed nuclear quadrupole frequencies for the nanomaterials studied, including bulk data for reference (open circles). The leftmost cluster is for anatase and TiO_2(B), whereas the other data points are for rutile (see text).

Ad i. and ii. First of all, it should be noted that none of the nanomaterials investigated is amorphous. On the contrary, all exhibit XRD reflexions, albeit broad, which allow the identification of the crystal structure unambiguously. For amorphous materials we would expect 2D-distributions of EFG tensor components, which would inevitably lead to non-zero average asymmetry parameters [20], contrary to observations.

A rather large linewidth of the volume signal implies that there is a wide distribution of inequivalent probe sites. This appears to be an intrinsic property of the nanomaterials and forms during the growth of the nanomaterials. A natural disorder in these materials would be a mixture of corner-sharing octahedra and edge-sharing octahedra where the O-excess is compensated by hydrogen atoms, not only at the surface but also in the volume. After all, what had been surface for a smaller particle will convert into volume when the particle grows.

The astonishing property for anatase and TiO_2(B) is the fact that despite the broad distributions in frequency (less so for TiO_2(B)) there is no significant indication of non-zero asymmetry parameters, the deviation from $\eta = 0$ is very small in any case. In other words, the O-octahedra have distortions, which either still have a four-fold rotation axis or a two-fold rotation-axis with a mirror-plane (like in anatase bulk). Since TiO_2(B) is a layered structure, it is apparently less prone to such disorder contrary to anatase, a 3D-structure.

Rutile, a metastable high-temperature structure, could be most prone to such disorder, as will be discussed in detail below. Here, the asymmetry parameter is close to unity in the bulk and we cannot exclude that the disorder would lead to a distribution in η and, hence, to an average η which is smaller than that of the bulk value. In this case, the argument with the broadened zero-frequency peak does not apply.

This type of disorder is rather stable since amorphous spark erosion samples with primary particle sizes around 5 nm converted to anatase (not rutile!) even at temperatures as high as 950°C and the ^{44}Ti-TDPAC volume signals were still rather broad [21]. So no further reduction of disorder takes place under these conditions. It could be that temperatures as high as 2/3 of the melting temperature would be required to remove the disorder. However, this is prohibitive because the nanomaterials would definitely sinter.

Ad iii. A common property for all materials studied is the fact that the surface signals are always sharper than the volume signals. There are two possible explanations: First, the hydrogen atom at the terminal OH-groups could be highly mobile, especially for larger undistorted terraces. The mobility is expected to be affected by steps, kinks, pores and alike. Secondly, the surface octahedra could be closer to being equivalent. Both effects probably play a role. In this respect the first-principles calculations of [6] which included water adsorption and OH-termination should be repeated with the possible inclusion of surface reconstructions.

Ad iv. The very small rutile particles (20 nm) are sort of a puzzle. Their volume signal is way off from the bulk value, contrary to their larger counterparts. In fact, this is the only case where this was observed. The signal is also far away from the anatase signal. Despite the fact that the XRD clearly indicates the rutile structure, there must be a large degree of disorder. This will be discussed below in more detail.

Nanowires. It is immediately obvious that the data for nanowires are easy to interpret because they exhibit two signals which are relatively sharp. We attribute the lower frequency with a fraction $f_1 = 73(4)\%$ to the volume fraction because of the similarity to the anatase bulk data. TiO_2(B) and anatase have similar volumes of the unit cell. This fraction can be estimated as follows: in a wire with a quadratic cross section of 3 nm and a length of 100 nm we have about 13,000 Ti-atoms; the surface is about 1,200 nm^2 and using an estimated Ti-OH distance of 0.25 nm we have about 4,500 near surface Ti-atoms; this gives a ratio of surface to volume atoms of 0.5 or 67% volume fraction. The higher frequency is then attributed to the surface where the sharpness of the signal indicates nearly perfect motional averaging due to highly mobile H-atoms on a nearly perfect surface. In fact, we expect a low degree of disorder and a smooth surface for the nanowires: defects

would probably lead to the termination of the wire growth keeping in mind that we have about 5 lattice spacings only for a 2 nm diameter. In addition the layered structure with the possibility to intercalate hydrogen atoms (probably ions, i.e. protons) is not prone to introduce disorder, the compound consists of outer and inner surfaces.

AMT-100 anatase. Similar assignments hold also true for AMT-100 (anatase, uncoated, 6 nm). The lower frequency, unfortunately much broader than that for the nanowires, is quite compatible with the anatase bulk value (about 18% higher) and we have axial symmetry. To our surprise, the higher frequency requires a substantial deviation from axial symmetry and is also substantially broadened, however less than the volume signal. The fractions are 78(6)% and 22(6)%, quite compatible with the estimated surface to volume ratio. This ratio can be estimated as follows: for anatase the unit cell volume is 0.136 nm^3 and in a cube of 6 nm length we have approximately 3,200 Ti-atoms; the surface is 216 nm^2 and using an estimated Ti-OH distance of 0.25 nm we have about 800 near surface Ti-atoms; this gives a ratio of surface to volume atoms of 0.3 or a volume fraction of 80%. The widths of the volume and the surface signals are distinctly wider than that for the nanowires. The finite asymmetry parameter indicates a different surface morphology than that of TiO_2(B) or it could be a hint for incomplete motional averaging. AMT-100 has a rather high BET-surface (280 m^2/g) and larger undistorted terraces are not expected.

2–4 nm anatase nanoparticles. The data for 2–4 nm anatase nanoparticles are least spectacular: we can fit the data with two fractions, the lower frequency with 8.7(6) Mrad/s and the higher one with 18(2) Mrad/s. The first signal has axial symmetry whereas the second signal requires a rather small but finite deviation from axial symmetry. Both are rather broad and the fractions depend sensitively on the line widths. Nevertheless, the fractions are close to 50%, as expected. The lower frequency is slightly lower compared to the anatase bulk value of 9.23(3) Mrad/s. The higher frequency is thus attributed to the surface signal. The widths of the volume and the surface signals are very broad, thus the disorder must be rather severe. It should be kept in mind that these nanoparticles were the only ones which were synthesized with the ^{44}Ti-activity added before synthesis and the material was dried at 37°C but not heated above 37°C.

Eusolex T-2000. The data for Eusolex T-2000 are distinctly different from the previous ones. First, we have the rutile modification. Second, the lanceolate particles have about 20 nm diameter and up to 100 nm length. Hence, the volume fraction must be the dominating fraction. In fact, a frequency $\omega_{Q,1}$ = 25.9(1.0) Mrad/s with η_1 = 0.64(2) is observed with a fraction f_1 = 88(4)%. For a rod with a quadratic cross-section and 20 nm width and an average length of 50 nm we would estimate a ratio for the surface to volume fraction of 6%, somewhat lower than the measured ratio but quite acceptable in view of the fact that the surface is rough. The surprise is that these NQI parameters deviate strongly from the rutile bulk data with ω_Q = 16.14(6) Mrad/s and η = 0.94(1) [10]. However, it should be kept in mind that the very large asymmetry parameter of 0.94 is observed for the Sc-impurity on the Ti-site only and not for Ti [22]. This could mean that this parameter is rather sensitive to details of the electronic structure, which in turn depend on surface termination and morphology. The mixture of edge- and corner-sharing octahedra – which is needed to understand the rather broad distributions – could also have a strong effect on the NQI parameters. It should be kept in mind that rutile is the metastable high-temperature modification and size effects could reduce the stability of the rutile modification. However, XRD measurements of Eusolex T-2000 confirmed the rutile structure. Hence, the electron distribution around the Sc-impurity seems to depend on particle size, on the degree of distortion, and on surface termination (Al_2O_3 coated!). The signal is comparatively sharp, hence the degree of distortion is not very high. This is certainly related to the particle morphology. The higher frequency must be attributed to the surface signal and is fairly sharp. However, there is again a marked deviation from axial symmetry which in this case is probably associated with the Al_2O_3-coating.

P25 rutile-extract. The data for the rutile-extract from P25 is somewhat easier to interpret because of extreme statistics. We required four fractions. The first component with a fraction f_1 = 60(10)% has hyperfine parameters comparable to those of bulk rutile, as expected for 85 nm

particles. The second fraction f_2 = 6(5)% is fairly sharp with δ_2 = 2(2)% and is tentatively assigned to the surface signal for the large particles. It is at the detection limit. The finite η_2 = 0.64(2) indicates that the surface termination of rutile is different from that of anatase, as expected. The second largest fraction f_3 resembles somehow the volume fraction of Eusolex T-2000, i.e. the 20 nm "rutile" particles, however η is different. A fit with larger η for this site resulted in a higher χ^2 and was discarded. The morphology of the Eusolex T-2000 particles differs significantly from that of the P25 rutile-extract (lanceolate versus globular) and it is not clear whether they adopt the same structure including distortions or not. The fourth fraction f_4 = 12(4)% is probably the surface signal of the smaller particles. This assignment is based on the expected surface to volume ratio. In fact, these parameters indicate that there are also rutile particles with much smaller size in the range of 20 nm, as was indeed observed in the SEM-image. As mentioned previously for Eusolex T-2000, the electron density distribution around the Sc-impurity seems to depend on particle size, degree of distortion, and surface termination. Note that none of the "surface" frequencies agrees with that of the surface signal of Eusolex T-2000, probably because of the Al_2O_3-coating of Eusolex T-2000. The surface fraction f_2 = 6(5)% is in agreement with the expectation for 85 nm particles. For a cube with 85 nm lengths we would estimate a surface fraction of a few percent only. The quoted BET-surface after the HF-treatment is 28 m^2/g [14] and roughly agrees with this surface fraction. Interestingly enough, whereas the SEM-image reveals that there is a broad distribution of particle sizes ranging from about 20 nm up to 100 nm, we observe relatively sharp signals. This supports the idea that the smaller particles do no longer have the undistorted rutile structure but adopt a different structure (e.g. rutile with a large amount of disorder) below a critical value, maybe around 50 nm. In any case, the small dampings δ_2 = 2(2)% and δ_4 = 2(1)% indicate a high surface quality for all particles.

Despite the fact that the data are very accurate and there is enough structure in the time spectrum and its cosine-transform, the data for all four sites have to be taken with some precaution except for the large particle fraction which is rather close to rutile bulk.

P25 (75% anatase, 25% rutile). The spectrum for P25 is rather complex. It is clear that most of the anisotropy is lost rapidly, i.e. the majority component has a rather broad frequency distribution, and there is a small almost undamped oscillatory component. Only after subtraction of the rutile signals as obtained from the P25 rutil-extract corresponding to a fraction of 25% [15], a spectrum which can be interpreted is obtained. We finally performed a fit with six components while keeping all rutile parameters (4 fractions, 4 deltas, 4 frequencies, 4 asymmetry parameters) fixed as obtained previously. This implies that the HF-treatment did not change the morphology of the rutile-extract. The results for the remaining anatase have to be taken with precautions because this assumption might not be fulfilled. The fitted frequency for the remaining anatase is ω = 9.6(7) Mrad/s with η = 0 fixed, slightly higher but in good agreement with the value for anatase bulk. However, the linewidth is excessively large which indicates a high degree of disorder. The surface fraction with f_2 = 4.4(2.5)% is on the low side to what is expected for 25 nm particles but still acceptable. For a 25 nm cube we estimate 230,000 atoms in the volume and 16,500 atoms near the surface which gives a surface to volume ratio of 0.07. The surface signal is amazingly sharp which indicates good surface quality.

Summary and Conclusions

In all nanomaterials studied thus far two different NQIs were observed which are assigned to probes in the volume and close to the surface, respectively. The only exception is the P25 rutile-extract which required separate pairs of signals for small and large particles. The volume and surface assignment is based on the following considerations:

(1) the volume signal must always be the dominant fraction with the only exception of the 2–4 nm nanoparticles;
(2) for anatase the NQI for the volume fraction resembles that of the bulk; for TiO_2(B) we have no bulk data but the similarity of the structure to anatase suggests that the NQI parameters should be similar; for rutile nanoparticles the NQI is much higher than that of the bulk and the asymmetry parameter is somewhat lower; however, there is no other choice;
(3) the second signal is always sharper than the volume signal, again with the exception of the 2–4 nm nanoparticles; this strongly suggests that mobile H-atoms which terminate the surface lead to partial or nearly complete motional averaging depending on the surface quality; in addition, the surface octahedra might be less prone to distortions; interestingly enough, the frequency ratio between surface to volume signal is 2–3 for anatase and TiO_2(B), whereas it is between 1.1 (small) and 1.5 (large) for rutile; we have no explanation for this fact (note that the line positions in the cosine-transforms depend on ω_Q and η, thus the lines do not coincide for the same ω_Q's if the η's are different);
(4) the corresponding fractions agree with expectations based on estimates about the number of Ti-atoms close to the surface with OH-termination relative to all other Ti-atoms.

In principle the high frequency fraction could also arise from undesired side reactions. However, we rule out this possibility because we would then lack a surface signal; moreover, the "surface" frequency is rather different for TiO_2(B)/anatase and rutile which would require different side reactions.

We can also exclude ferromagnetic order in our samples for the following reasons: first, magnetic moments associated with unpaired electrons at defects are not expected under the growth conditions with O and H supply; next, ferromagnetic order would result in a perturbation function with two spectral features of the same strength, one of the Larmor frequency and one with twice the Larmor frequency, which was never observed. For the very small particles we would anyway expect superparamagnetism, i.e. fluctuating magnetic fields which – combined with the NQI – would yield relaxation-type spectra, which was never observed.

As far as the degree of distortions is concerned we would rank the nanomaterials as follows based on the line broadening of the volume fraction:

P25 rutile-extract < wires ~ Eusolex T-2000 < AMT-100 anatase < 2–4 nm nanoparticles < P25 anatase.

A low degree of distortion should be synonymous with good photocatalytic activity because the mean free path for electrons is large enough such that they can all reach the surface, at least for very small particles. However, it is unclear what the mean free path of electrons would be in a 5 nm particle with distortions.

As far as surface quality is concerned, we would rank the nanomaterials as follows based on the linebroadening of the surface fraction:

P25 rutile-extract ~ P25 anatase > wires ~ Eusolex T-2000 > AMT-100 anatase > 2–4 nm nanoparticles.

Good surface quality should be synonymous with good catalytic activity because highly mobile H-atoms should be easily exchangeable. This mobility would also be supported by surface octahedra lacking distortions; however, this correspondence is not really clear.

It should be kept in mind that Eusolex T-2000 is coated with Al_2O_3 and thus the surface signal might not arise from Ti with OH-bonds but rather from ^{44}Ti in the Al_2O_3-layer and is thus not directly comparable. The quoted amount of Al_2O_3 in the technical data sheet would be compatible with this assignment.

With all precautions concerning the assignment and interpretation of the volume and surface signals we nevertheless want to stress the following results which are pertinent for the characterization of the nanomaterials apart from structure, size, size distribution, morphology, surface termination, and stoichiometry:

a) static properties: there is a variable degree of distortion of the octahedra which we consider to be due to intrinsic defects arising from a mixture of corner- and edge-sharing octahedra; e.g. connecting two octahedra instead of three via corners would lead to O-excess which can be compensated by hydrogen atoms;
b) dynamic properties: the partial or full motional averaging of the NQI-signals due to mobile H-atoms on the surface has not yet been accounted for adequately.

Acknowledgment

It is a pleasure to thank Mrs. A. Setzer for the XRD measurements, Prof. Dr. Th. Höche and Dr. G. Wagner for the HRTEM images, and J. Lenzner for the SEM images. The AMT-100 material was kindly provided by Dr. J. Lekki and the P25 from Prof. Dr. D. Enke.

References

[1] Xiao Chen and Samuel S. Mao, Chem. Rev. Vol. 107 (2007), p. 2891.

[2] R. Marchand, L. Brohan, and M. Tournoux, Mater. Res. Bull. Vol. 15 (1980), p. 1129.

[3] S. Eiden-Assmann, J. Widoniak, and G. Maret, Chem. Mater. Vol. 16 (2004), p. 6.

[4] P. Krüger, S. Bourgeois, B. Domenichini, H. Magnan, D. Chandesris, P. Le Fèvre, A. M. Flank, J. Jupille, L. Floreano, A. Cossaro, A. Verdini, and A. Morgante, Phys. Rev. Lett. Vol. 100 (2008), p. 055501.

[5] Shengqiang Zhou, E. Čižmár, K. Potzger, M. Krause, G. Talot, M. Helm, J. Fassbender, S. A. Zryagin, J. Wosnitza, and H. Schmidt, Phys. Rev. B Vol. 79 (2009), p. 113201.

[6] Xue-Qing Gong, A. Selloni, M. Batzill, and U. Diebold, Nat. Mater. Vol. 5 (2006), p. 665.

[7] www.tayca.co.jp/english.

[8] www.merck-chemicals.com.

[9] corporate.evonik.com.

[10] S.-b. Ryu, S. K. Das, T. Butz, W. Schmitz, Ch. Spiel, P. Blaha, and K. Schwarz, Phys. Rev. B Vol. 77 (2008), p. 094124.

[11] D. Bahnemann, A. Henglein, J. Lilie, and L. Spanhel, J. Phys. Chem. Vol. 88 (1984), p. 709.

[12] A. A. Gribb and J. F. Banfield, Am. Mineral. Vol. 82 (1997), p. 717.

[13] G. H. Lee and J.-M. Zuo, J. Am. Ceram. Soc. Vol. 87 (2004), p. 473.

[14] Songwang Yang and Lian Gao, Chem. Lett. Vol. 34 (2005), p. 972.

[15] T. Ohno, K. Sarukawa, K. Tojieda, and M. Matsumura, J. Catal. Vol. 203 (2001), p. 82.

[16] R. B. Firestone, *Table of Isotopes*, 8th ed., Wiley, New York (1996).

[17] F. E. Wietfeldt, F. J. Schima, B. M. Coursey, and D. D. Hoppes, Phys. Rev. C Vol. 59 (1999), p. 528.

[18] T. Butz, Hyperfine Interact. Vol. 52 (1989), p. 189.

[19] G. Czjzek, Hyperfine Interact. Vol. 14 (1984), p. 189.

[20] T. Butz, Physica Scripta Vol. 78 (2008), p. 015801.

[21] W. G. Kreyling, P. Biswas, M. E. Messing, N. Gibson, M. Geiser, A. Wenk, M. Sahu, K. Deppert, I. Cydzik, Ch. Wigge, O. Schmidt, and M. Semmler-Behnke, J.Nanopart. Res. DOI 10.1007/s11051-010-0081-5; T. Butz et al. (to be published)

[22] O. Kanert and H. Kolem, J. Phys. C Vol. 21 (1988), p. 3909.